Integrated Fast Assembly of Free-Standing Lithium Titanate/Carbon Nanotube/Cellulose Nanofiber Hybrid Network Film as Flexible Paper-Electrode for Lithium-Ion Batteries

Shaomei Cao,[†] Xin Feng,*[,†] Yuanyuan Song,[§] Xin Xue,[†] Hongjiang Liu,[‡] Miao Miao,[†] Jianhui Fang,[‡] and Liyi Shi[†,‡]

[†]Research Center of Nano Science and Technology, Shanghai University, 99 Shangda Road, Shanghai 200444, P. R. China
[‡]Department of Chemistry, College of Science, Shanghai University, Shanghai 200444, P. R. China
[§]School of Materials Sciences and Engineering, Shanghai University, Shanghai 200444, P. R. China

Ⓢ Supporting Information

ABSTRACT: A free-standing lithium titanate $(Li_4Ti_5O_{12})$/carbon nanotube/cellulose nanofiber hybrid network film is successfully assembled by using a pressure-controlled aqueous extrusion process, which is highly efficient and easily to scale up from the perspective of disposable and recyclable device production. This hybrid network film used as a lithium-ion battery (LIB) electrode has a dual-layer structure consisting of $Li_4Ti_5O_{12}$/carbon nanotube/cellulose nanofiber composites (hereinafter referred to as LTO/CNT/CNF), and carbon nanotube/cellulose nanofiber composites (hereinafter referred to as CNT/CNF). In the heterogeneous fibrous network of the

hybrid film, CNF serves simultaneously as building skeleton and a biosourced binder, which substitutes traditional toxic solvents and synthetic polymer binders. Of importance here is that the CNT/CNF layer is used as a lightweight current collector to replace traditional heavy metal foils, which therefore reduces the total mass of the electrode while keeping the same areal loading of active materials. The free-standing network film with high flexibility is easy to handle, and has extremely good conductivity, up to 15.0 S cm^{-1}. The flexible paper-electrode for LIBs shows very good high rate cycling performance, and the specific charge/discharge capacity values are up to 142 mAh g^{-1} even at a current rate of 10 C. On the basis of the mild condition and fast assembly process, a CNF template fulfills multiple functions in the fabrication of paper-electrode for LIBs, which would offer an ever increasing potential for high energy density, low cost, and environmentally friendly flexible electronics.

KEYWORDS: cellulose nanofiber, free-standing fibrous network film, flexible paper-electrode, pressure-controlled extrusion process, lithium-ion batteries
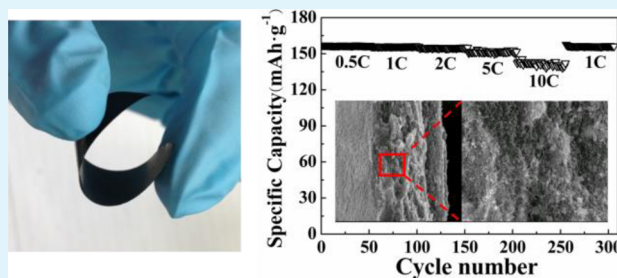
INTRODUCTION

There is a growing interest in thin, lightweight, environmentally friendly, flexible, and even foldable energy storage devices to meet the special needs for next-generation, high-performance, flexible electronics,[1] such as soft portable electronic products, roll-up displays, wearable devices, implantable biomedical devices, and conformable health-monitoring electronic skin.[2,3] Rechargeable lithium-ion batteries (LIBs) have been considered as the most promising dominant power source and energy storage system for a vast range of portable electronics.[4,5] Nevertheless, two issues that need to be addressed for future production of flexible LIBs still remain. First, the most widely used fluorine-based binders (e.g., poly(vinylidene fluoride)) for electrode fabrication are expensive and usually require the use of volatile and toxic organic solvents such as *N*-methyl pyrrolidone,[6] which lead to safety problems upon cycling[7,8] and the difficulty of electrode disposal at the end of the LIB's life.[9,10] Second, LIBs electrodes based on metal substrates (e.g.,

Cu and Al foil) as current collectors will increase the mass of the LIBs and thus decrease the energy density and capacity density.[11] Moreover, the weak adhesion of metal substrate and electrode material results in invalidation of flexible LIBs under the condition of repeated bending or folding. Therefore, the important requirement for ideal alternatives to supplant traditional components of LIBs electrodes as quickly as possible is becoming an increasingly more and more significant trend.[11−15]

Carbon nanotube (CNT) thin films with high conductivity and flexibility[16] coated on cellulose paper[17] or plastic substrates[18] have been used as current collectors to replace heavy metal foils in LIBs and supercapacitors (SCs). Due to its renewability, biodegradability and biocompatibility, cellulose is

emerging as a perfect candidate for synthetic polymers in assembly of flexible electronics. Recently, the preparation of electrodes for LIBs and SCs using cellulose,[19] carboxymethyl cellulose (CMC),[20−25] or CMC combined with other natural polymers[26] as binders has been carried out. Of importance is that cellulose acting as substrates[17,27,28] or binders[29,30] will pave the way for the large scale production of eco-friendly flexible LIB electrodes. Jabbour et al.[31] prepared low cost, self-standing, and flexible LiFePO$_4$/carbon black powder/cellulose fibers paper-cathodes by means of an eco-friendly, water-based filtration process, and cellulose fibers represented a valid biosourced alternative to synthetic binders. Leijonmarck et al.[32] described a vacuum sequential filtration method for production of paper-based LIBs cells in which nanofibrillated cellulose acted as binder material as well as load-bearing material. However, mimetic paper-making process for assembly of paper-electrode such as water evaporation and vacuum filtration usually require several hours to a few days; the difficulty is the extremely slow dewatering because of the high water binding capacity of cellulose fiber.[33,34]

Cellulose nanofiber (CNF) extracted from abundant renewable native plant fiber has excellent properties, including being lightweight and having a high elastic modulus[35] and a low thermal expansion,[36] making them an ideal building block to host a range of guest materials for the fabrication of a new type of flexible electrodes. In this study, we developed a free-standing flexible paper-electrode using CNF as both building skeleton and a biosourced binder, Li$_4$Ti$_5$O$_{12}$ (LTO) nanoparticles as active material, CNT as electronic conductivity enhancer without using any organic solvents. A fast pressure-controlled aqueous extrusion method was successfully applied for fabricating the free-standing LTO/CNT/CNF hybrid network film. This hybrid network film has a dual-layer structure consisting of LTO/CNT/CNF and CNT/CNF; here, the CNT/CNF fibrous layer with a thickness of about 10 μm is utilized as a current collector replacing the traditional metal substrate. The integrated design of hybrid film combines the advantages of LTO, CNT, and CNF, and increases the adhesion and contact area between the CNT/CNF current collector and LTO/CNT/CNF active material. CNF combined with CNT constructs a robust conductive fibrous network, and CNT linked with LTO aims to build electronic conductive paths to help remedy the intrinsically low electronic conductivity of LTO.[37,38] Furthermore, the obtained paper-electrode with high flexibility can be redispersed in water at the end of the battery life as common paper sheets, which is extremely interesting from the perspective of easily recyclables and eco-friendly device production.

■ EXPERIMENTAL SECTION

Materials. Li$_4$Ti$_5$O$_{12}$ (LTO) powders with particle size of 100−200 nm were synthesized in the laboratory according to our previous literature,[39] which has several advantages: high theoretical capacity (ca. 175 mA h g^{-1}),[40] small volumetric change (ca. 0.2%),[41] and a potential of approximately 1.56 V (free of the reductive electrolyte decomposition).[42] Cellulose nanofiber (CNF) with fiber diameter of 20−30 nm and aspect ratios of 20−200 was extracted after the chemical cleavage of the amorphous region of kelp residues[43] by a high-pressure homogenization process (D−3L, PhD Technology LLC).[43,44] Carbon nanotube (CNT) aqueous dispersion (solid content: 4%) with diameter 30−50 nm and length 5−12 μm was provided by Shenzhen Susn Sinotech New Materials Co., Ltd. Sodium dodecyl benzenesulfonate (SDBS) and glycerol used as dispersion stabilizer and plasticizer, respectively, were purchased from Sinopharm

Chemical Reagent Co., Ltd. Lithium hexafluorophosphate (LiPF$_6$), ethylene carbonate (EC), and diethyl carbonate (DEC) electrolyte were purchased from Zhangjiagang Guotai Huarong New Chemical Material Co., Ltd.

Preparation of LTO/CNT/CNF Conductive Slurries. First, CNT aqueous dispersion was diluted with deionized water to a lower concentration of 0.1% (w/w), and SDBS was added to obtain an equally dispersed solution by mechanical stirring for 30 min. At the same time, another aqueous suspension containing 0.1% w/w CNF was prepared by dilution and sonication (power 200 W) in 10 °C water bath for about 30 min. Then, CNF suspension with a certain amount of glycerol (used to improve the film forming ability) was added into the CNT aqueous with CNT:CNF in mass ratio 2:1; thus, the CNT/CNF composite suspensions were obtained after ultrasonic treatment at the same condition for about 30 min. Finally, different amounts of LTO dispersions (0.3‰ w/w) were added into the CNT/CNF composite suspension with sonication under the same condition to form LTO/CNT/CNF mixed conductive slurries with LTO percentage of 50%, 60%, and 70%.

Fast Assembly of Free-Standing Flexible Paper-Electrode. Free-standing flexible network film with a dual-layer was assembled by two steps of the pressure-controlled aqueous extrusion process as shown the schematic illustration in Figure 1. The conductive slurry
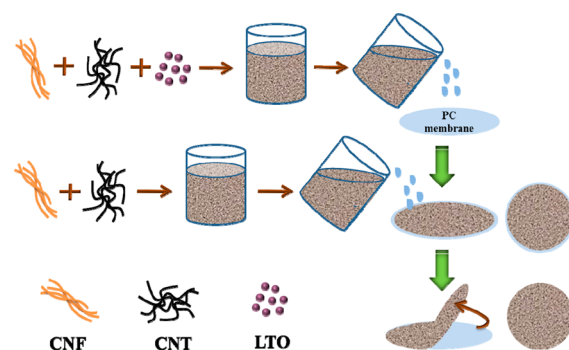

Figure 1. Schematic illustration of fast assembly of free-standing flexible hybrid film.

containing LTO, CNT, and CNF was first poured into the extruder (NanoAble-150, PhD Technology LLC) and filtrated through a PC membrane (nuclepore track-etch membrane, pore size 200 nm, Whatman) under a controlled pressure of 1.0 MPa, then the CNT/CNF composite suspension containing CNT and CNF was filtrated onto the bottom layer, and the whole process took only about 1 h. The dual-layer film with the PC membrane was subsequently sandwiched between two glass sheets and dried at 95 °C under vacuum for 15 min. The free-standing flexible network film for the paper-electrode was finally obtained after separating from the PC membrane easily.

Characterization. The morphology of LTO, CNT, and CNF in the suspension was observed using a field emission transmission electron microscope (FETEM) (JEM-2010F, JEOL, Japan). The surface and cross section topography of the film were imaged using a field emission scanning electron microscope (FESEM) (JSM-6700F, JEOL, Japan). X-ray diffraction (XRD) patterns (D/max 2550, Rigaku, Japan) were taken to detect the different components in the hybrid film. Electronic conductivity was measured using the standard four probe technique (RTS-8, China), and the measurements were averaged on 3 replicates.

Electrochemical Measurements. The electrochemical properties of the paper-electrode were measured by a two-electrode electrochemical cell at ambient temperature (25 °C). First, the obtained LTO/CNT/CNF network films with different LTO percentages were dried at 100 °C under high vacuum environment for 24 h to ensure complete water removal, and then were cut into disks with diameter of 15 mm. The coin half-cells were assembled in an argon-filled glovebox (O$_2$ and H$_2$O content <0.5 ppm) using Li-foil as counter electrode, Celgard 2400 as separator, and 1 M LiPF$_6$ in a 1:1 (volume) mixture of
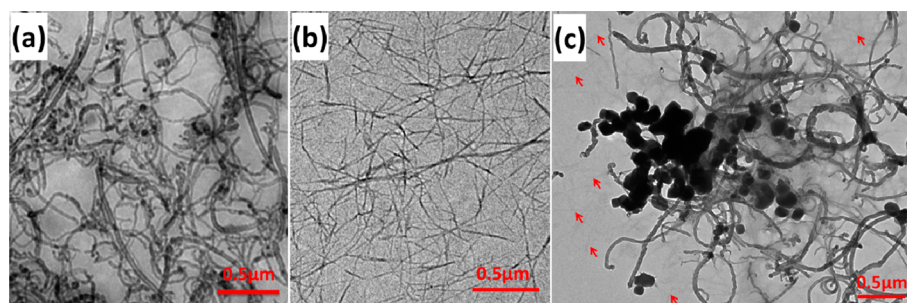
Figure 2. TEM images of (a) CNT and (b) CNF aqueous suspension and (c) LTO/CNT/CNF conductive slurry.

EC and DEC as the electrolyte. The cells were tested at various current densities using a LAND-CT2001A cell test instrument in a voltage window of 1.0−2.5 V (vs Li/Li$^+$) at room temperature (25 °C). Cycle voltammograms (CV) were recorded from 0.8 to 2.5 V at a scanning rate of 0.2 mV s^{-1} using a CHI660D Electrochemical Workstation, and the electrochemical impedance spectra were measured by CHI660D impedance analyzer in the frequency range from 10 mHz to 100 kHz with a potential perturbation at 5 mV. All the LIB measurements mentioned above are based on the mass of LTO in the electrode. The paper-electrodes with different LTO percentages of 50%, 60%, and 70% are referred to as LCC-50, LCC-60, and LCC-70 in the following.

■ RESULTS AND DISCUSSION

Figure 2a,b shows the TEM images of CNT and CNF aqueous suspension, respectively. It can be clearly seen that the CNT and CNF are highly dispersed and all are found to be nanometric in diameter. In the TEM image of the LTO/CNT/CNF conductive slurry (Figure 2c), the LTO particles are coagulated on the surface of CNT, which will result in a high increase in the conductivity of LTO. CNF can be seen blurry (marked by red arrows) in the image for its smaller size and deficient crystallinity compared to CNT and LTO. Due to the high water binding capacity, CNF was used as dispersing stabilizer in LTO/CNT/CNF conductive slurry to avoid LTO agglomeration and to improve the film homogeneity.[45]

Figure 3a shows the digital photos of the fast assembled free-standing network film and inset illustrating high flexibility of the film. The flexible film with smooth surface is easy to handle, and the diameter of the film is about 42 mm; the thickness is about 35 μm controlled by the mass of the filtration slurry. In Figure 3b, FESEM image of the bottom layer containing LTO, CNT, and CNF composites indicates that LTO particles are dispersed in CNT and CNF hybrid fibrous network. The CNT/CNF fibrous network embeds and consolidates LTO particles to form a free-standing network film and simultaneously acts as electronic conductive paths to help remedy the intrinsically low electronic conductivity of LTO. In Figure 3c, the FESEM image of the top layer containing CNT and CNF acted as a current collector shows that the fibers intertwined together and formed a compact network structure with large pores which can allow the electrolyte to diffuse into it easily. Figure 3d−f shows the cross section of the dual-layer film. From Figure 3d, the thickness of the film is well-determined (∼35 μm) as shown in the picture, and the cross section morphology shows two well-adhering layers comprising CNT/CNF and LTO/CNT/CNF. CNF is an ideal platform for bridging the current collector and active materials. Figure 3e,f reveals the zoomed-in images of the interface between the dual-layer as shown in Figure 3d, indicating that CNT/CNF fibers partly penetrated into the LTO/CNT/CNF layer caused by the
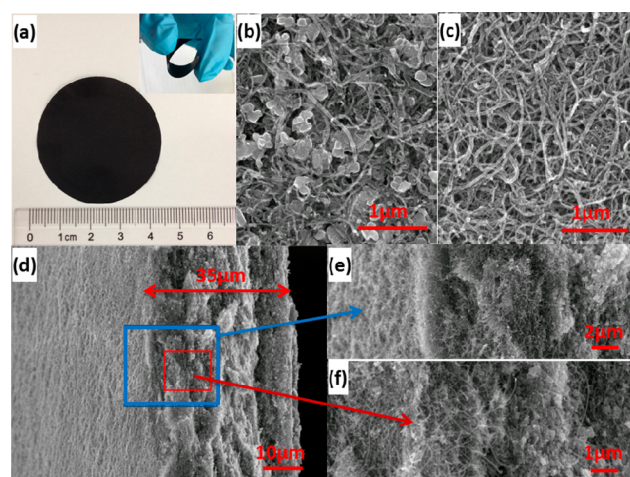

Figure 3. (a) Digital photos of the obtained free-standing network film and inset illustrating the flexibility of the film. (b) FESEM image of the bottom layer containing LTO, CNT, and CNF composites. (c) FESEM image of the top layer containing CNT and CNF network. (d) FESEM image of the cross section of the dual-layer film. (e) Zoomed-in image of the cross section, as in the blue box in part d. (f) Zoomed-in image of the cross section, as in the red box in part d.

extrusion process, and this will dramatically enhance the electronic conductivity of the paper-electrode.

XRD measurements were performed to determine the different components of the hybrid film. The XRD pattern of LTO powders, CNT film, CNF film, and LTO/CNT/CNF film are shown in Figure 4, respectively. It is obvious that the LTO/CNT/CNF film contains the characteristic peaks of
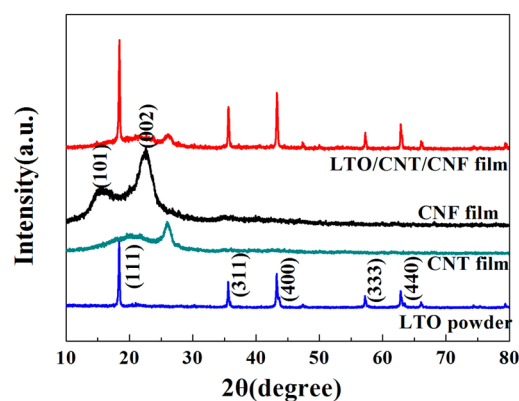

Figure 4. XRD patterns of LTO powders, CNT film, CNF film, and the final LTO/CNT/CNF hybrid film.

LTO, CNT, and CNF. Some minor characteristic peaks of CNF in LTO/CNT/CNF film are nearly invisible for the lower percentage of CNF in the final hybrid film, and the initial peak intensity is relatively weaker. The stronger peaks in the final composite film are ascribed to well-crystallized LTO with cubic spinel structure (JCPDS Card 49-0207).

The use of CNT and CNF leads to the elaboration of paper-electrode with optimal conductivity and structure properties. The electron conductivities of the hybrid films were measured using the standard four probe technique as shown in Figure 5.
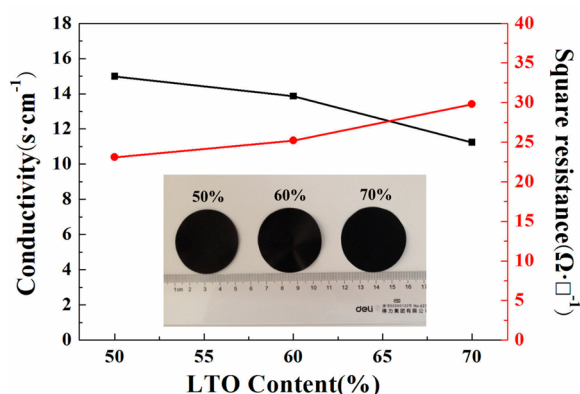

Figure 5. Conductivity and square resistance of the hybrid films (inset: digital photos of LCC-50, LCC-60, and LCC-70).

The square resistance of LCC-50 is about 23 Ω sq^{-1}, equal to the electronic conductivity, which is about 15.0 S cm^{-1}. With the increasing of LTO percentages to 60% and 70%, the conductivity of LCC-60 and LCC-70 is decreased to about 13.8 and 11.2 S cm^{-1}, respectively. When the LTO percentage is increased higher than 80%, the soundness of the hybrid film

was destroyed, and lots of network cracks were formed (Figure S1a, Supporting Information). This could be ascribed to the introduction of too many rigid LTO particles onto the flexible CNT/CNF fibrous network, so that the extent of interfibril hydrogen bonding in CNF was reduced,[46] resulting in agglomeration of LTO and consequent breaking of film integrity. As the comparison, the hybrid films without CNF or CNT were also fabricated, respectively. However, LTO/CNT film without CNF was hardly separated from the PC membrane (Figure S1b, Supporting Information), and the resistance of LTO/CNF film without CNT was too large to be tested by ohmmeter (Figure S2b, Supporting Information). The results indicated that a proper proportion of LTO, CNT, and CNF was beneficial to design a LTO/CNT/CNF hybrid film with a given electronic conductivity and mechanical integrity for paper-electrode.

CNT/CNF film without LTO as paper-electrode for LIBs was investigated in coin half-cells versus Li-foil from 1.0 to 2.5 V in order to evaluate the contribution of CNT to the capacity (Figure S3, Supporting Information). The results indicated that the discharge capacity of a CNT/CNF electrode is about 3 mA h g^{-1}, which can be negligible compared to the capacity of ca. 160 mA h g^{-1} for the LTO/CNT/CNF electrode. Figure 6 compared the rate capability of the fast assembled LTO/CNT/CNF paper-electrode with different LTO percentage (LCC-50, LCC-60, and LCC-70). The rate performances of LCC-50, LCC-60, and LCC-70 cycled at current rates ranging from 0.5 to 10 C (each sustained for 50 cycles, 1 C = 175 mA h g^{-1}) and are shown in Figure 6a; a very stable cycling ability was observed for LCC-50 at each current rate. The paper-electrodes deliver a high specific capacity of 157, 154, and 150 mA h g^{-1} for LCC-50, LCC-60, and LCC-70 at 0.5 C, respectively. With the current rates increasing to 5 and 10 C, LCC-50 still delivers a capacity of 152 and 142 mA h g^{-1}, and still has a capacity
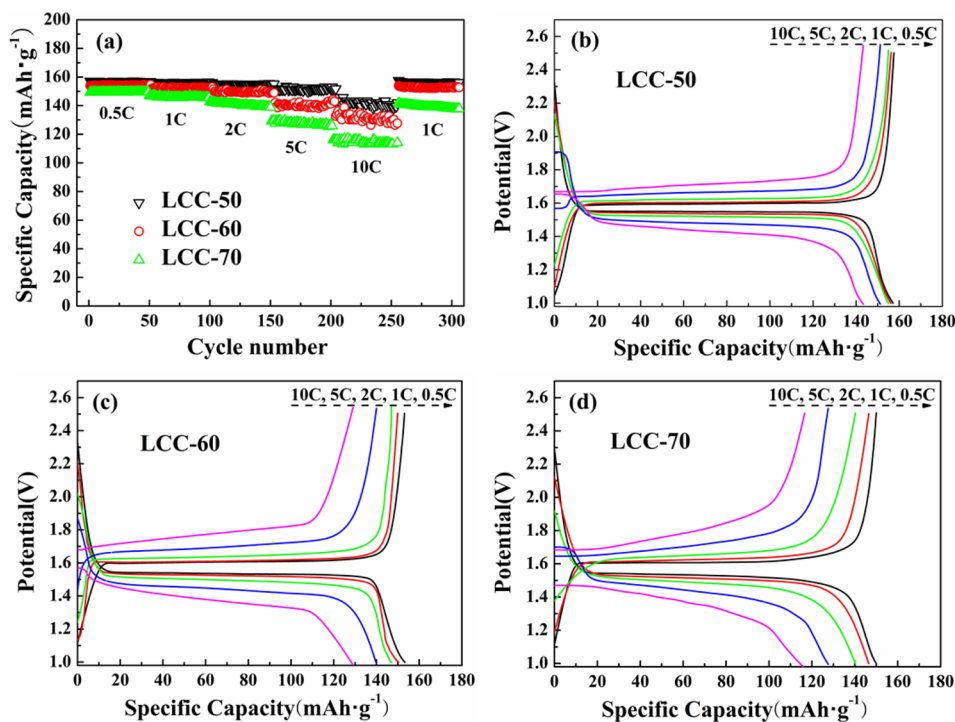

Figure 6. (a) Rate performance of LCC-50, LCC-60, and LCC-70. Galvanostatic charge/discharge curves of (b) LCC-50, (c) LCC-60, and (d) LCC-70 at different current rates.
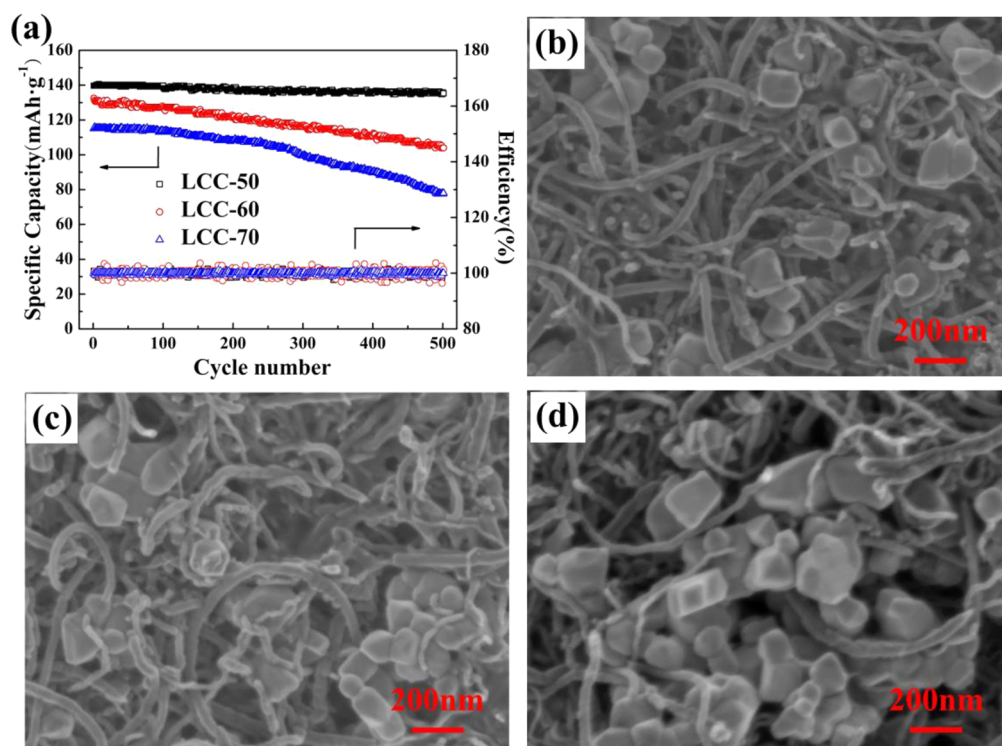
Figure 7. (a) Cycling performance of LCC-50, LCC-60, and LCC-70 at current rate of 10 C (left: specific capacity; right: Coulombic efficiency). FESEM images of (b) LCC-50, (c) LCC-60, and (d) LCC-70 after cycling at 10 C for 500 cycles.
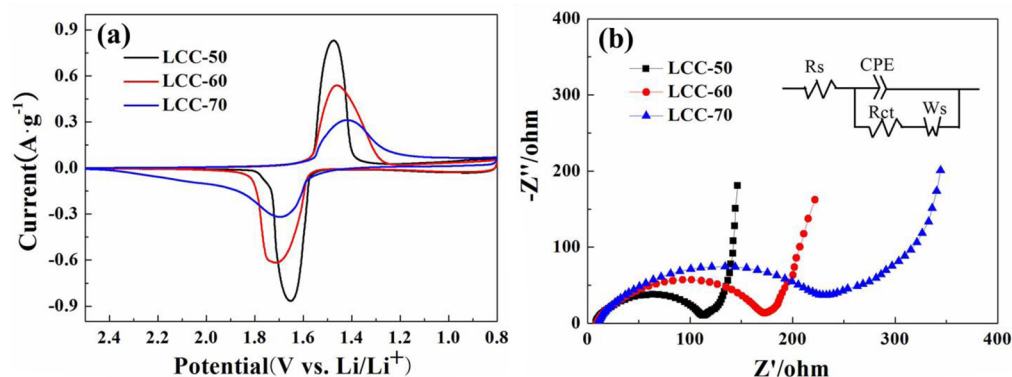

Figure 8. (a) Cyclic voltammogram of LCC-50, LCC-60, and LCC-70 at a scanning rate of 0.2 mV s^{-1} in a voltage window 0.8−2.5 V. (b) Electrochemical impedance spectroscopy of LCC-50, LCC-60, and LCC-70 electrodes; the inset shows the equivalent circuit.

retention of 96.8% and 90.4% of the initial capacity at 0.5 C, respectively. The good reversibility of LTO-50 is demonstrated by the fact that the capacity of 156 mA h g^{-1} is almost completely recovered when reducing the rate back to 1 C again, whereas, for LCC-60 and LCC-70, further increasing LTO percentage leads to a drop in rate capability and low specific capacity retention, especially at higher current rates from 5 to 10 C. It can be concluded that the rate performance of LCC-50 was much better than those of LCC-60 and LCC-70. Figure 6b−d show the typical galvanostatic charge/discharge curves of LCC-50, LCC-60, and LCC-70 at different current rates from 0.5 to 10 C, respectively. It is obvious that the difference between charge and discharge potentials of LCC-50 is less than those of LCC-60 and LCC-70, especially at high rates, implying that LCC-50 has clearly lower charge/discharge polarization. All the charge/discharge curves appear as a long flat platform corresponding to the Li$^+$ ion insertion/deinsertion process in

the LTO framework. For LCC-50, when the current rate increased to 10 C, the discharge capacity decreased gradually from 157 to 142 mA h g^{-1}, and the charge/discharge voltage plateau became shorter. For LCC-60 and LCC-70, the discharge capacity decreased to 129 and 115 mA h g^{-1}, and the charge/discharge voltage plateau gradually bent down with the increase of charge−discharge rates. This potential difference probably resulted from the polarization degree of LCC-50, LCC-60, and LCC-70.[47] The LCC-50 electrode exhibits the higher rate capability maybe due to its better electronic conductivity,[48] which is consistent with that of Figure 5.

Cycling stability is an important parameter for rating LIBs; the cycling performances of the paper-electrodes at 10 C are shown in Figure 7. It can be seen from Figure 7a that LCC-50 exhibited stable cycling performance and higher capacity retention ratio than those of LCC-60 and LCC-70 after 500 cycles. The initial capacities of LCC-50, LCC-60, and LCC-70

are 140, 131, and 115 mA h g^{-1}, respectively. After 500 cycles, the obtained capacity retention is 96.4% for LCC-50, 79.4% for LCC-60, and 68.8% LCC-70, respectively. In addition, the Coulombic efficiency is nearly 100% for all the samples. The excellent cycling performance of LCC-50 can be attributed to the perfect heterogeneous network architectures with a proper amount of LTO. In LTO/CNT/CNF nanocomposites, the intercalation of LTO in voids generated by the loose packing of CNT and CNF enhances the electrochemical reactivity of the paper-electrode. Moreover, CNT fibrous webs serve as channels for electron transportation, while large numbers of pores on their surface provide transport channels for Li$^+$ ions.[49] The paper-electrodes of LCC-50, LCC-60, and LCC-70 after cycling at 10 C for 500 cycles show an indistinguishable morphological difference (Figure 7b−d). The paper-electrodes still remain a relative structural integrity and no occurrence of microcracks can be seen from the low amplification FESEM images (Figure S4, Supporting Information). The result indicates that the electrochemical process has no additional impact on the paper-electrode structure during cycling.

Figure 8a showed cyclic voltammogram (CV) of LCC-50, LCC-60, and LCC-70 at a scanning rate of 0.2 mV s^{-1} in a potential window of 0.8−2.5 V. A couple of characteristic redox peaks of the LCC-50 paper-electrode are illustrated at about 1.66 and 1.50 V, corresponding to the Li$^+$ ions deinsertion and insertion of LTO. It can be found that the redox peaks are narrower and sharper than those of LCC-60 and LCC-70, which implies that LCC-50 possesses faster reaction kinetics, higher rate performance, and less polarization. Electrochemical impedance spectroscopy (EIS) was one of the most sensitive tools to compare the charge transfer resistances of LCC-50, LCC-60, and LCC-70. The EIS and its impedance equivalent circuit are shown in Figure 8b. According to the equivalent circuit (inset in Figure 8b), the diameter of the semicircle in the high frequency region is mainly related to the charge transfer resistance (R_{ct}). The R_{ct} values of LCC-50, LCC-60, and LCC-70 are 110, 175, and 230 Ω, respectively, fitted by Zview software,[50] which is significantly lower than that of a previous report.[39] The results further proved that, along with the increase of LTO percentage in the paper-electrode, the electronic conductivity was decreased. The proper amounts of CNT and LTO have a significant effect on the elaboration of an efficient conductive network in LTO/CNT/CNF composites.

CONCLUSION

In summary, a pressure-controlled aqueous extrusion process has been utilized for the fast assembly of a free-standing LTO/CNT/CNF hybrid film. The integrated effect from the bilayer of the CNT/CNF current collector and LTO CNT/CNF active material was in favor of constructing a heterogeneous fibrous network with ease-of-fabrication and a close combination for a flexible paper-electrode. The free-standing hybrid film demonstrated good potential as a flexible paper-electrode in LIBs with excellent electrochemical properties, such as high charge/discharge capacities, high rate performance, and stable cycling performance. Moreover, CNF extracted from kelp residue was used both as building skeleton and biosourced binder for the paper-electrode. The assembled paper-electrode without use of volatile or toxic organic solvents can be redispersed in water at the end of the battery life as common paper sheets, which are easily recyclable and eco-friendly for the environment.

ASSOCIATED CONTENT

Ⓢ Supporting Information

Photograph of LTO/CNT/CNF film with LTO percentage of 80%. Photograph of LTO/CNT film on a PC membrane. Poor conductivity of LTO/CNF film without CNT. Galvanostatic charge/discharge curves of CNT/CNF film and LTO/CNT/CNF film from 1.0 to 2.5 V. Low-magnification FESEM images of (a) LCC-50, (b) LCC-60, and (c) LCC-70 after 500 cycles at 10 C. The Supporting Information is available free of charge on the ACS Publications website at DOI: 10.1021/acsami.5b02693.

AUTHOR INFORMATION

Corresponding Author
*E-mail: fengxin@shu.edu.cn.

Notes
The authors declare no competing financial interest.

ACKNOWLEDGMENTS

REFERENCES

(1) Rogers, J. A.; Someya, T.; Huang, Y. Materials and Mechanics for Stretchable Electronics. *Science* **2010**, *327*, 1603−1607.

(2) Nishide, H.; Oyaizu, K. Toward Flexible Batteries. *Science* **2008**, *319*, 737−738.

(3) Tarascon, J. M.; Armand, M. Issues and Challenges Facing Rechargeable Lithium Batteries. *Nature* **2001**, *414*, 359−367.

(4) Etacheri, V.; Marom, R.; Elazari, R.; Salitra, G.; Aurbach, D. Challenges in the Development of Advanced Li-ion Batteries: a Review. *Energy Environ. Sci.* **2011**, *4*, 3243−3262.

(5) Scrosati, B.; Garche, J. Lithium Batteries: Status, Prospects and Future. *J. Power Sources* **2010**, *195*, 2419−2430.

(6) Yoshio, M.; Brodd, R. J.; Kozawa, A. *Lithium-Ion Batteries: Science and Technologies*; Springer: New York, 2009.

(7) Maleki, H.; Deng, G.; Kerzhner-Haller, I.; Anani, A.; Howard, J. N. Thermal Stability Studies of Binder Materials in Anodes for Lithium-Ion Batteries. *J. Electrochem. Soc.* **2000**, *147*, 4470−4475.

(8) Markevich, E.; Salitra, G.; Aurbach, D. Influence of the PVdF Binder on the Stability of LiCoO₂ Electrodes. *Electrochem. Commun.* **2005**, *7*, 1298−1304.

(9) Nnorom, I. C.; Osibanjo, O. Heavy Metal Characterization of Waste Portable Rechargeable Batteries Used in Mobile Phones. *Int. J. Environ. Sci. Technol.* **2009**, *6*, 641−650.

(10) Xu, J.; Thomas, H. R.; Francis, R. W.; Lum, K. R.; Wang, J.; Liang, B. A Review of Processes and Technologies for the Recycling of Lithium-ion Secondary Batteries. *J. Power Sources* **2008**, *177*, 512−527.

(11) Wang, K.; Luo, S.; Wu, Y.; He, X.; Zhao, F.; Wang, J.; Jiang, K.; Fan, S. Super-Aligned Carbon Nanotube Films as Current Collectors for Lightweight and Flexible Lithium Ion Batteries. *Adv. Funct. Mater.* **2013**, *23*, 846−853.

(12) Song, S.; Kim, S. W.; Lee, D. J.; Lee, Y.-G.; Kim, K. M.; Kim, C.-H.; Park, J.-K.; Lee, Y. M.; Cho, K. Y. Flexible Binder-Free Metal Fibril Mat-Supported Silicon Anode for High-Performance Lithium-Ion Batteries. *ACS Appl. Mater. Interfaces* **2014**, *6*, 11544−11549.

(13) Zhu, G.; Wang, Y.; Xia, Y. Ti-based Compounds as Anode Materials for Li-ion Batteries. *Energy Environ. Sci.* **2012**, *5*, 6652−6667.

(14) Chen, H.; Xiao, Y.; Wang, L.; Yang, Y. Silicon Nanowires Coated with Copper Layer as Anode Materials for Lithium-ion Batteries. *J. Power Sources* **2011**, *196*, 6657−6662.

(15) Braun, P. V.; Cho, J.; Pikul, J. H.; King, W. P.; Zhang, H. High Power Rechargeable Batteries. *Curr. Opin. Solid State Mater. Sci.* **2012**, *16*, 186−198.

(16) Hu, L.; Hecht, D. S.; Gruner, G. Percolation in Transparent and Conducting Carbon Nanotube Networks. *Nano Lett.* **2004**, *4*, 2513−2517.

(17) Hu, L.; Choi, J. W.; Yang, Y.; Jeong, S.; Mantia, F. L.; Cui, L.; Cui, Y. Highly Conductive Paper for Energy-Storage Devices. *Proc. Natl. Acad. Sci. U.S.A.* **2009**, *106*, 21490−21494.

(18) Kaempgen, M.; Chan, C. K.; Ma, J.; Cui, Y.; Gruner, G. Printable Thin Film Supercapacitors Using Single-Walled Carbon Nanotubes. *Nano Lett.* **2009**, *9*, 1872−1876.

(19) Sen, U. K.; Mitra, S. High-Rate and High-Energy-Density Lithium-Ion Battery Anode Containing 2D MoS_2 Nanowall and Cellulose Binder. *ACS Appl. Mater. Interfaces* **2013**, *5*, 1240−1247.

(20) Kim, G. T.; Jeong, S. S.; Joost, M.; Rocca, E.; Winter, M.; Passerini, S.; Balducci, A. Use of Natural Binders and Ionic Liquid Electrolytes for Greener and Safer Lithium-ion Batteries. *J. Power Sources* **2011**, *196*, 2187−2194.

(21) Lee, J.-H.; Kim, J.-S.; Kim, Y. C.; Zang, D. S.; Paik, U. Dispersion Properties of Aqueous-Based $LiFePO_4$ Pastes and Their Electrochemical Performance for Lithium Batteries. *Ultramicroscopy* **2008**, *108*, 1256−1259.

(22) Lee, J.-H.; Kim, J.-S.; Kim, Y. C.; Zang, D. S.; Choi, Y.-M.; Park, W., II; Paik, U. Effect of Carboxymethyl Cellulose on Aqueous Processing of $LiFePO_4$ Cathodes and Their Electrochemical Performance. *Electrochem. Solid-State Lett.* **2008**, *11*, A175−A178.

(23) Li, J.; Klöpsch, R.; Nowak, S.; Kunze, M.; Winter, M.; Passerini, S. Investigations on Cellulose-Based High Voltage Composite Cathodes for Lithium Ion Batteries. *J. Power Sources* **2011**, *196*, 7687−7691.

(24) Lux, S. F.; Schappacher, F.; Balducci, A.; Passerini, S.; Winter, M. Low Cost, Environmentally Benign Binders for Lithium-Ion Batteries. *J. Electrochem. Soc.* **2010**, *157*, A320−A325.

(25) Xie, L.; Zhao, L.; Wan, J.; Shao, Z.; Wang, F.; Lv, S. The Electrochemical Performance of Carboxymethyl Cellulose Lithium as a Binding Material for Anthraquinone Cathodes in Lithium Batteries. *J. Electrochem. Soc.* **2012**, *159*, A499−A505.

(26) Buqa, H.; Holzapfel, M.; Krumeich, F.; Veit, C.; Novák, P. Study of Styrene Butadiene Rubber and Sodium Methyl Cellulose as Binder for Negative Electrodes in Lithium-Ion Batteries. *J. Power Sources* **2006**, *161*, 617−622.

(27) Hu, L.; Wu, H.; Cui, Y. Printed Energy Storage Devices by Integration of Electrodes and Separators into Single Sheets of Paper. *Appl. Phys. Lett.* **2010**, *96*, 183502−1−183502−3.

(28) Wolfenstine, J.; Lee, U.; Allen, J. L. Electrical Conductivity and Rate-Capability of $Li_4Ti_5O_{12}$ as a Function of Heat-Treatment Atmosphere. *J. Power Sources* **2006**, *154*, 287−289.

(29) Hu, L.; Mantia, F. L.; Wu, H.; Xie, X.; Donough, J. M.; Pasta, M.; Cui, Y. Lithium-Ion Textile Batteries with Large Areal Mass Loading. *Adv. Energy Mater.* **2011**, *1*, 1012−1017.

(30) Nyström, G.; Mihranyan, A.; Razaq, A.; Lindström, T.; Nyholm, L.; Strømme, M. A Nanocellulose Polypyrrole Composite Based on Microfibrillated Cellulose from Wood. *J. Phys. Chem. B* **2010**, *114*, 4178−4182.

(31) Pushparaj, V. L.; Shaijumon, M. M.; Kumar, A.; Murugesan, S.; Ci, L.; Vajtai, R.; Linhardt, R. J.; Nalamasu, O.; Ajayan, P. M. Flexible Energy Storage Devices Based on Nanocomposite Paper. *Proc. Natl. Acad. Sci. U. S. A.* **2007**, *104*, 13574−13577.

(32) Leijonmarck, S.; Cornell, A.; Lindbergh, G.; Wågberg, L. Single-Paper Flexible Li-ion Battery Cells through a Paper-Making Process Based on Nano-fibrillated Cellulose. *J. Mater. Chem. A* **2013**, *1*, 4671−4677.

(33) Österberg, M.; Vartiainen, J.; Lucenius, J.; Hippi, U.; Seppälä, J.; Serimaa, R.; Laine, J. A Fast Method to Produce Strong NFC Films as a Platform for Barrier and Functional Materials. *ACS Appl. Mater. Interfaces* **2013**, *5*, 4640−4647.

(34) Huang, W.; Ouyang, X.; Lee, L. High-Performance Nanopapers Based on Benzenesulfonic Functionalized Graphenes. *ACS Nano* **2012**, *6*, 10178−10185.

(35) Jabbour, L.; Destro, M.; Chaussy, D.; Gerbaldi, C.; Penazzi, N.; Bodoardo, S.; Beneventi, D. Flexible Cellulose/$LiFePO_4$ Paper-Cathodes: Toward Eco-Friendly All-Paper Li-Ion Batteries. *Cellulose* **2013**, *20*, 571−582.

(36) Iwamoto, S.; Kai, W.; Isogai, A.; Iwata, T. Elastic Modulus of Single Cellulose Microfibrils from Tunicate Measured by Atomic Force Microscopy. *Biomacromolecules* **2009**, *10*, 2571−2576.

(37) Fergus, J. W. Recent Developments in Cathode Materials for Lithium Ion Batteries. *J. Power Sources* **2010**, *195*, 939−954.

(38) Fröschl, T.; Hörmann, U.; Kubiak, P.; Kučerová, G.; Pfanzelt, M.; Weiss, C. K.; Behm, R. J.; Hüsing, N.; Kaiser, U.; Landfester, K.; Wohlfahrt-Mehrens, M. High Surface Area Crystalline Titanium Dioxide: Potential and Limits in Electrochemical Energy Storage and Catalysis. *Chem. Soc. Rev.* **2012**, *41*, 5313−5360.

(39) Cheng, C.; Liu, H.; Xue, X.; Cao, H.; Shi, L. Highly Dispersed Copper Nanoparticle Modified Nano $Li_4Ti_5O_{12}$ with High Rate Performance for Lithium Ion Battery. *Electrochim. Acta* **2014**, *120*, 226−230.

(40) Fukuzumi, H.; Saito, T.; Iwata, T.; Kumamoto, Y.; Isogai, A. Transparent and High Gas Barrier Films of Cellulose Nanofibers Prepared by TEMPO-Mediated Oxidation. *Biomacromolecules* **2009**, *10*, 162−165.

(41) Jung, H. G.; Venugopal, N.; Scrosati, B.; Sun, Y. K. A High Energy and Power Density Hybrid Supercapacitor Based on an Advanced Carbon-Coated $Li_4Ti_5O_{12}$ Electrode. *J. Power Sources* **2013**, *221*, 266−271.

(42) Shen, L.; Yuan, C.; Luo, H.; Zhang, X.; Chen, L.; Li, H. Novel Template-Free Solvothermal Synthesis of Mesoporous $Li_4Ti_5O_{12}$-C Microspheres for High Power Lithium Ion Batteries. *J. Mater. Chem.* **2011**, *21*, 14414−14416.

(43) Miao, M.; Zhao, J. P.; Feng, X.; Cao, Y.; Cao, S. M.; Zhao, Y. F.; Ge, X. Q.; Sun, L. N.; Shi, L. Y.; Fang, J. H. Fast Fabrication of Transparent and Multi-Luminescent TEMPO-Oxidized Nanofibrillated Cellulose Nanopaper Functionalized with Lanthanide Complexes. *J. Mater. Chem. C* **2015**, *3*, 2511−2517.

(44) Zhao, J. P.; Wei, Z. W.; Feng, X.; Miao, M.; Sun, L. N.; Cao, S. M.; Shi, L. Y.; Fang, J. H. Luminescent and Transparent Nanopaper Based on Rare-Earth Up-Converting Nanoparticle Grafted Nanofibrillated Cellulose Derived from Garlic Skin. *ACS Appl. Mater. Interfaces* **2014**, *6*, 14945−14951.

(45) Li, Y.; Zhu, H.; Shen, F.; Wan, J.; Lacey, S.; Fang, Z.; Dai, H.; Hu, L. Nanocellulose as Green Dispersant for Two-Dimensional Energy Materials. *Nano Energy* **2015**, DOI: 10.1016/j.nanoen.2015.02.015.

(46) Liu, A.; Walther, A.; Ikkala, O.; Belova, L.; Berglund, L. A. Clay Nanopaper with Tough Cellulose Nanofiber Matrix for Fire Retardancy and Gas Barrier Functions. *Biomacromolecules* **2011**, *12*, 633−641.

(47) Shi, Y.; Wen, L.; Li, F.; Cheng, H. M. Nanosized $Li_4Ti_5O_{12}$/ Graphene Hybrid Materials with Low Polarization for High Rate Lithium Ion Batteries. *J. Power Sources* **2011**, *196*, 8610−8617.

(48) Zhang, Z. H.; Zhou, Z. F.; Nie, S.; Wang, H. H.; Peng, H. R.; Li, G. C.; Chen, K. Z. Flower-like Hydrogenated $TiO_2(B)$ Nanostructures as Anode Materials for High-Performance Lithium Ion Batteries. *J. Power Sources* **2014**, *267*, 388−393.

(49) Qie, L.; Chen, W. M.; Wang, Z. H.; Shao, Q. G.; Li, X.; Yuan, L. X.; Hu, X. L.; Zhang, W. X.; Huang, Y. H. Nitrogen-Doped Porous Carbon Nanofiber Webs as Anodes for Lithium Ion Batteries with a Superhigh Capacity and Rate Capability. *Adv. Mater.* **2012**, *24*, 2047−2050.

(50) Yang, T.; Sang, L.; Ding, F.; Zhang, J.; Liu, X. Three- and Four-Electrode EIS Analysis of Water Stable Lithium Electrode with Solid Electrolyte Plate. *Electrochem. Acta* **2012**, *81*, 179−185.